Comparative study of the alloying effect on the initial oxidation of Cu-Au(100) and Cu-Pt(100)

Langli Luo, Yihong Kang, Judith C. Yang, Dong Su, Eric A. Stach, and Guangwen Zhou

Citation: Applied Physics Letters **104**, 121601 (2014); doi: 10.1063/1.4870085
View online: http://dx.doi.org/10.1063/1.4870085
View Table of Contents: http://scitation.aip.org/content/aip/journal/apl/104/12?ver=pdfcov
Published by the AIP Publishing

Comparative study of the alloying effect on the initial oxidation of Cu-Au(100) and Cu-Pt(100)

Langli Luo,[1] Yihong Kang,[2] Judith C. Yang,[3] Dong Su,[4] Eric A. Stach,[4] and Guangwen Zhou[1,a)]
[1]*Department of Mechanical Engineering and Multidisciplinary Program in Materials Science and Engineering, State University of New York, Binghamton, New York 13902, USA*
[2]*Department of Mechanical Engineering and Materials Science, University of Pittsburgh, Pittsburgh, Pennsylvania 15261, USA*
[3]*Department of Chemical and Petroleum Engineering, University of Pittsburgh, Pittsburgh, Pennsylvania 15261, USA*
[4]*Center for Functional Nanomaterials, Brookhaven National Laboratory, Upton, New York 11973, USA*

(Received 1 January 2014; accepted 20 March 2014; published online 27 March 2014)

Using *in situ* transmission electron microscopy, we show that the oxidation of the Cu-Au(100) results in the formation of Cu_2O islands that deeply embed into the Cu-Au substrate while the oxidation of the Cu-Pt(100) leads to the formation of Cu_2O islands that highly protrude above the Cu-Pt substrate. Their difference is attributed to the different mobilities of Pt and Au in the Cu base alloys for which the sluggish mobility of Pt in Cu results in trapped Pt atoms at the oxide/alloy interface while the faster mobility of Au in Cu leads to enhanced rehomogenization of the alloy composition. © *2014 AIP Publishing LLC*. [http://dx.doi.org/10.1063/1.4870085]

Copper and copper alloys are important materials which are often used under the conditions where surface oxidation strongly affects their properties and functionalities. For instance, Cu is widely used as an interconnection material in the fabrication of integrated circuits because of its low resistivity and high resistance to electron migration. A typical 45/65 nm logic technology incorporates nine/eight Cu interconnect layers[1,2] and also utilizes the Cu-Au alloy as the liner. Significant changes in mechanical and electrical properties can occur through surface alloying and interface degradation resulting from oxidation.[3] Therefore, the environmental stability of Cu base alloys becomes a crucial problem when the dimensions of these devices shrink to the nanoscale. Cu and Cu alloys are also widely used in the chemical industry including Cu-based catalysts for a wide variety of catalytic reactions such as methanol oxidation and steaming reforming.[4–6] For these chemical processes, a critical issue is related to the surface oxidation of Cu that may significantly modify the reactivity/selectivity of Cu-based catalysts.[7]

Oxidation of metals typically involves hierarchical multiple length scales starting from oxygen surface chemisorption to oxide nucleation and growth and then to the formation of a continuous oxide layer. The nucleation and growth of oxide islands, which are not considered in the traditional oxidation theories, play a critical role in the structure and composition evolution of the oxide film. In general, alloy oxidation is much more complex than pure metals due to the convolution of different effects such as different oxygen affinities of the alloying elements, formation of multiple oxide phases, and various mobilities of metals in the oxide and alloy. As such, the understanding of early-stage oxidation of alloys is still significantly unclear. The oxidation of Cu has been a rich source of information for understanding oxide nucleation and growth.[8–14] To elucidate the effect of alloying on oxide island formation, we perform an *in situ* transmission electron microscopy (TEM) study of the early-stage oxidation of Cu-Au and Cu-Pt alloys. These two systems are chosen for comparative study since they allow for examining some features of alloy oxidation without the complication of simultaneous formation of multiple oxides because Au and Pt do not oxidize under most conditions.[15]

The oxidation experiments were performed in a modified JEL200CX TEM equipped to allow observation of oxidation in real time. Cu-10 at. %Au(100) and Cu-10 at. %Pt(100) thin films with ~500 Å thickness were grown on NaCl(100) by e-beam evaporation. The alloy films were then removed from the substrate by floatation in deionized water and mounted on a TEM specimen holder. A leak valve attached to the TEM column permits introduction of gases directly into the TEM with a controlled oxygen gas pressure (pO_2). Before oxidation experiments, native oxide can be removed by annealing in the TEM chamber at 750 °C under vacuum condition[16] or *in situ* annealing under H_2 gas at pressure $\sim 10^{-5}$ Torr and 350 °C, resulting in a clean surface. The sample cleanliness was checked by electron diffraction. Oxygen gas of 99.999% purity was then admitted into the column of the microscope through the leak valve to oxidize clean alloy films at a constant temperature and oxygen pressure pO_2. *In situ* TEM observations of the oxidation process were made in planar views. Cu forms two thermodynamically stable oxides, CuO and Cu_2O. For the temperature and low oxygen pressure employed in our experiments, only Cu_2O is expected to form. This was confirmed by electron diffraction analysis during the *in situ* TEM observation of the oxidation.[17,18] To identify the spatial distribution of elements (i.e., O, Cu, Au, and Pt) in the oxidized Cu-Au and Cu-Pt samples, scanning transmission electron microscopy (STEM) energy dispersive X-ray spectroscopy (EDX) elemental mapping was performed using a Hitachi HD2700 (200 kV) with a probe aberration-corrector.

a)Author to whom correspondence should be addressed. Electronic mail: gzhou@binghamton.edu

Fig. 1(a) shows time-resolved bright-field (BF) TEM images captured from the real-time video (see multimedia view of Fig. 1(a)) monitoring the growth of an oxide island during the oxidation of a Cu-10 at. %Au(100) surface at $T = 450\,^{\circ}C$ and $pO_2 = 5 \times 10^{-4}$ Torr. The oxide has the Cu_2O phase and shows cube-on-cube epitaxial growth with the alloy substrate as identified by selected area electron diffraction (SAED) pattern shown in Fig. 1(a). An incubation time is needed before the formation of a visible oxide embryo after oxygen gas is introduced into the microscope. As seen in Fig. 1, an area with slightly dark contrast appears first and it then evolves into a larger triangle-shaped dark region during the incubation period. After ~2 min of oxidation, the profile of a round-shaped oxide island becomes clearly visible at the center of the dark-contrast zone. The size and shape of the dark-contrast zone remains relatively unchanged after the oxide island is formed. The oxide island grows laterally, catching and passing the dark-contrast area. While the oxide island still remains an overall round shape during the growth, the island edge becomes partly faceted at a larger size, as marked in Fig. 1(a) at the oxidation time $t = 400$ s and 600 s. The evolution of the lateral size of the oxide island is measured from the *in situ* TEM video and is plotted as a function of oxidation time (Fig. 1(b)). A linear growth behavior is noted, and the growth rate is ~2265 nm^2/s. We also measured the oxidation at 650 °C and a similar linear growth behavior but with a faster growth rate (~4146 nm^2/s) is observed, as shown in Fig. 1(b).

Fig. 2(a) shows *in situ* TEM images extracted from the real-time video (see multimedia view of Fig. 2(a)) of the oxidation of a Cu-10 at. %Pt(100) surface at $T = 450\,^{\circ}C$ and $pO_2 = 5 \times 10^{-4}$ Torr. The *in situ* TEM observation reveals that the Cu-Pt(100) surface has a slower oxidation rate than the Cu-Au(100), i.e., a longer incubation time is needed to form a clearly visible oxide embryo followed by a slower growth rate of the oxide island. Different from Cu-Au(100), the Cu-Pt(100) surface does not show the formation of a dark-contrast area during the incubation period. After a visible Cu_2O island is formed, the entire island appears much darker than the surrounding area. The oxide island develops into a truncated triangle shape with faceted edges. The oxide island has the Cu_2O phase and is cube-on-cube epitaxial with the Cu-Pt substrate, as shown by the electron diffraction pattern obtained from the oxide island (Fig. 2(a)). Similar measurement is made on the lateral size of the oxide island and Fig. 2(b) shows its size evolution as a function of time. It can be noted that the oxide island on the Cu-Pt(100) surface also

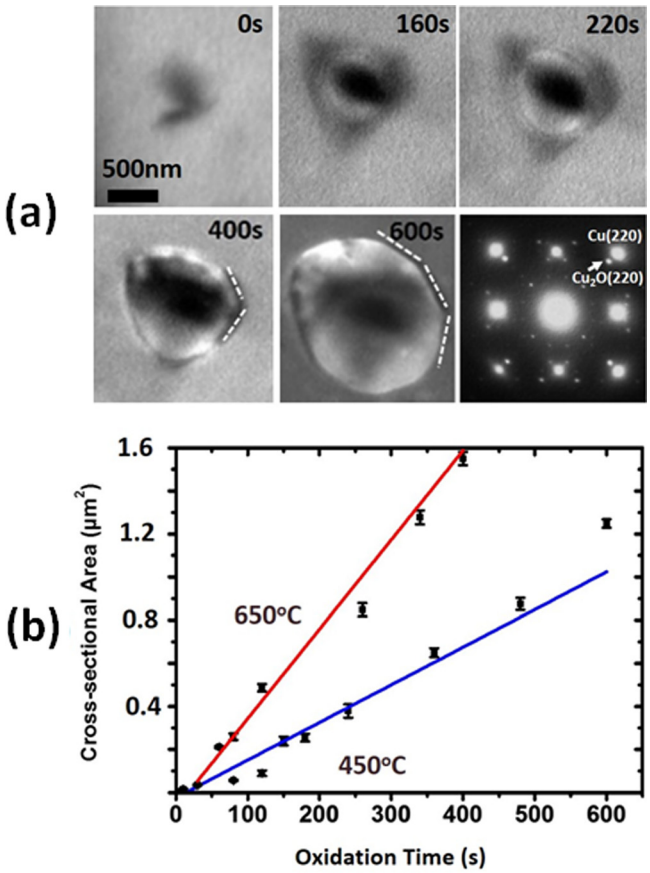

FIG. 1. (a) *In situ* TEM observation of the growth of a Cu_2O island on Cu-10 at. %Au(100) during the oxidation at $T = 450\,^{\circ}C$ and $pO_2 = 5 \times 10^{-4}$ Torr. Inset is an SAED pattern revealing the epitaxial oxide growth with the substrate. The oxide island initially shows a round shape and gradually develops into a faceted shape (indicated by dashed lines) with the continued oxidation. (b) Evolution of the lateral size of the oxide island as a function of oxidation time. (Multimedia view) [URL: http://dx.doi.org/10.1063/1.4870085.1]

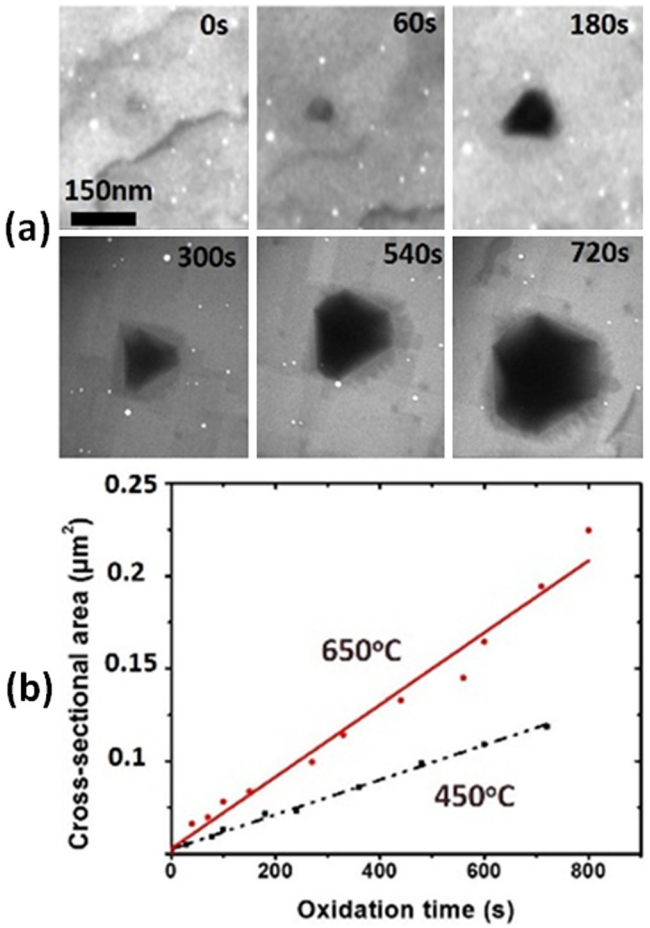

FIG. 2. (a) *In situ* TEM observation of the growth of a Cu_2O island on Cu-10 at. %Pt(100) during the oxidation at $T = 450\,^{\circ}C$ and $pO_2 = 5 \times 10^{-4}$ Torr. Inset is an SAED pattern revealing the epitaxial oxide growth with the substrate. The oxide island initially has a faceted triangle shape and develops into a truncated triangle polygon with the continued oxidation. (b) Evolution of the lateral size of the oxide island as a function of oxidation time. (Multimedia view) [URL: http://dx.doi.org/10.1063/1.4870085.2]

shows a linear growth behavior with a rate of ~376 nm^2/s, which is much slower than that for the oxide island on the Cu-Au(100) surface. Such a linear growth behavior is also observed from the Cu-Pt(100) oxidation at 650 °C with a faster growth rate of 802 nm^2/s (Fig. 2(b)).

STEM EDX elemental mapping was employed to examine the composition distribution of the oxidized samples. Fig. 3(a) shows a BF-STEM image of an oxide island formed on the Cu-10 at. %Au(100) surface oxidized at T = 450 °C and $pO_2 = 5 \times 10^{-4}$ Torr, where the island edges are highly faceted. Figs. 3(b)–3(d) show Cu, O, and Au elemental mappings of the oxide island and its surrounding alloy region. O is accumulated within the oxide island (Fig. 3(d)) while Cu shows a lower intensity in the oxide area compared to the surrounding alloy region (Fig. 3(b)), suggesting that the Cu_2O island grows deep into the alloy thin film by consuming Cu atoms in the alloy underneath the oxide island (note that the concentration of Cu in Cu_2O is less than that of the Cu-base alloy). The Au mapping (Fig. 3(c)) shows that the un-oxidized alloy region has a much higher intensity than the oxide region, revealing that Au atoms are expelled laterally into the alloy during the oxide growth and becomes enriched in the surrounding alloy.

Similar EDX mapping was also performed on the Cu-10 at. %Pt(100) sample oxidized at 450 °C and $pO_2 = 5 \times 10^{-4}$ Torr, as shown in Figs. 3(f)–3(i). Fig. 3(f) shows an annular dark-field STEM (i.e., mass-contrast) image of three oxide islands formed on the Cu-Pt(100) surface. The smaller Cu_2O island still shows a truncated triangle shape while the larger islands have developed into a nearly square shape. Here, the much brighter contrast from the oxide islands suggests that the total thickness in these regions is much thicker than the surrounding area. As expected, O is enriched in the oxide region (Fig. 3(i)). However, different from the Cu-Au(100) surface where Cu is less concentrated in the oxide island region than the surrounding alloy and Au is enriched laterally in the surrounding alloy; Figs. 3(g) and 3(h) reveal that Cu shows a much stronger intensity in the oxide region than the surrounding alloy, while the Pt intensity is relatively uniform across the entire sample region. The stronger Cu intensity in the oxide region suggests that the oxide islands do not embed deep into the alloy film, thereby retaining Cu atoms in the alloy underneath the oxide islands. Surprisingly, Fig. 3(h) reveals that Pt has a uniform intensity across the entire surface, a clear evidence that Pt is not expelled laterally during the oxide growth (i.e., Pt becomes enriched at the oxide/alloy interface). Since the oxide islands do not grow into the substrate, the 3D Cu_2O island growth protruding above the surface is sustained by depletion of Cu atoms from the surrounding alloy, which results in an overall uniform enrichment of Pt across the entire surface region (and thus uniform intensity of Pt mapping).

Figs. 3(e) and 3(j) illustrate schematically the difference in the oxide growth induced element segregation in the Cu-Au and Cu-Pt alloys based the EDX analysis. For the Cu-Au alloy, the lateral enrichment of Au atoms in the surrounding alloy allows the oxide island to grow deeply into the alloy. For the Cu-Pt alloy, the enrichment of Pt atoms in the oxide/alloy interface area suppresses the oxide from growing into the alloy substrate, alternatively, the oxide island increases its thickness via protruding above the alloy surface with the supply of Cu atoms depleted from the surface region of the surrounding alloy. Their difference between Cu-Au and Cu-Pt can be also confirmed from the BF TEM image contrast feature as revealed in Figs. 1 and 2, where the Cu_2O island grown on the Cu-Au surface shows bright contrast while the oxide island on the Cu-Pt surface shows dark contrast. For BF TEM imaging, the bright contrast corresponds to a more open structure than the surrounding area, and the dark contrast corresponds to a more dense structure (or larger thickness) than the surrounding area. Cu_2O has a lattice con-

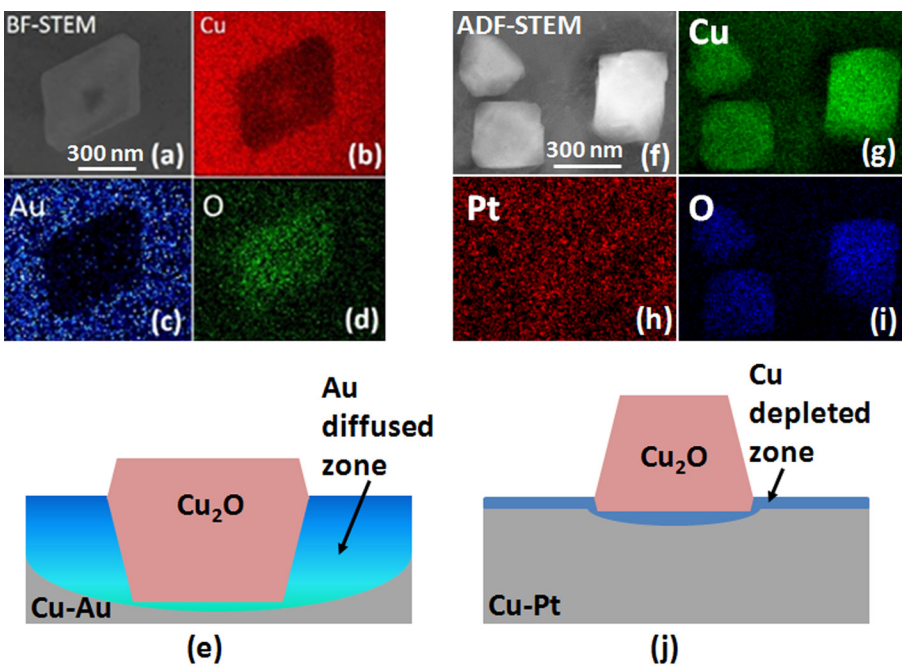

FIG. 3. EDX elemental mapping of oxide islands formed on (a)–(d) Cu-10 at. %Au(100) and (f)–(j) Cu-10 at. %Pt(100) under the condition of 450 °C and $pO_2 = 5 \times 10^{-4}$ Torr. (e) and (j) Show schematic of oxide growth model on two alloy, respectively.

stant of 4.22 Å and its structure is more open than the Cu-10 at. %Au alloy ($a_{Cu\text{-}10at.\%Au} \sim 3.61$ Å). The appearance of bright contrast for the oxide island on the Cu-Au alloy suggests that the oxide island grows into the substrate by consuming denser Cu-Au alloy beneath. The dark contrast for Cu_2O islands on the Cu-Pt alloy suggests that the oxide island protrudes above the surface without significantly embedding into the Cu-Pt substrate, which results in a much larger total thickness (alloy film plus oxide island height) compared to the oxide islands from the oxidation of the Cu-Au alloy.

The difference in the oxidation induced redistribution of Au and Pt can be attributed to the different mobilities of Au and Pt in the Cu-Au and Cu-Pt alloys. Due to their stable electronic configurations, both Au and Pt do not go into solution in the oxide phase. Therefore, the oxidation of the Cu-Au and Cu-Pt alloys results in rejection of Au and Pt from the metal/oxide interface, leading to Au and Pt enrichment in the remaining Cu-Au and Cu-Pt alloys, respectively. The activation energy for bulk diffusion of Pt in Cu is ~1.51 eV,[19] while the value for bulk diffusion of Au in Cu is ~1.1 eV.[20] Thus, Pt atoms rejected from the oxide growth during the oxidation of the Cu-Pt alloy remain in the alloy adjacent to the oxide-alloy interfacial area due to the sluggish mobility of Pt atoms. In contrast, Au atoms rejected from oxide growth during the oxidation of the Cu-Au alloy can diffuse away from the oxide-alloy interface region and spread out from the metal-oxide interface, as schematically illustrated in Figs. 3(e) and 3(j). This also explains why the Cu-Au alloy initially develops a dark-contrast zone in the *in situ* TEM images (shown in Fig. 1) due to the spreading of Au atoms from the oxide nucleation location and subsequent building up in the surrounding alloy region. The oxidation of the Cu-Pt alloy does not show such a behaviour because Pt atoms expelled from the oxide growth are trapped at the oxide-alloy interface from the beginning.

Their difference in the 3D oxide islanding can be also evidenced from *ex situ* atomic force microscopy (AFM) measurements on the surface topology of the oxide islands formed on the two alloys. Fig. 4 shows AFM tomographic images of the two alloys oxidized under the same condition of T = 450 °C and $pO_2 = 5 \times 10^{-4}$ Torr. For the Cu_2O island formed on the Cu-Au(100) surface, the line profiles reveal a maximum island height of 0.16 μm and a lateral size of ~2 μm, with a height/width aspect ratio of ~0.08. The oxide island grown on the Cu-Pt(100) surface has a smaller lateral size of ~1.5 μm but a larger height of ~0.47 μm (i.e., a height/width aspect ratio of ~0.31). The AFM measurements indicate that the oxide island on the Cu-Pt surface shows more prominent 3D growth. This is because the trapped Pt atoms at the oxide/alloy interface suppress the oxide growth into the substrate, which in turn promotes the oxide growth as protrusion above the substrate surface via surface diffusion of Cu atoms from the surrounding alloy. It can be also noted from the AFM images in Fig. 4 that the area adjacent to the oxide island on the Cu-Au surface is sunken deeply while it is much less for the oxide island on the Cu-Pt surface. This sunken area is formed as a result of the embedment of the oxide island into the Cu-Au substrate.

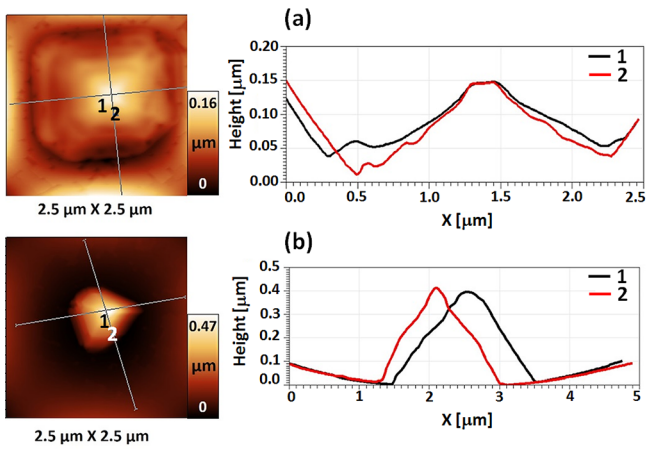

FIG. 4. AFM topological images of oxide nuclei formed on (a) Cu-5 at. %Au(100) and (b) Cu-5 at. %Pt(100) under the condition of 450 °C and $pO_2 = 5 \times 10^{-4}$ Torr for 10 min.

In conclusion, using *in situ* TEM observations of the initial-stage oxidation of the Cu-Au(100) and Cu-Pt(100) alloys, we show that the oxide growth modes are closely related to the diffusivity of the noble elements in the alloys. The oxidation of the Cu-Au alloys results in formation of Cu_2O islands that highly embed into the Cu-Au substrate due to the fast diffusion of Au in Cu while the oxidation of the Cu-Pt alloy leads to the formation of Cu_2O islands that highly protrude above the Cu-Pt substrate surface due to the sluggish mobility of Pt in Cu that suppresses the oxide islands from embedding into the substrate. These results demonstrate the necessity of incorporating the effect of atom mobility in alloy design for manipulating the initial oxide growth. These results may also have broader implications, such as in alloy design or heterogeneous catalysis, for which element surface segregation of an alloy under reactive environments often occurs but the interplay between the thermodynamic driving force and the atom mobility is still not very clear.

Research was supported by the U.S. Department of Energy, Office of Basic Energy Sciences, Division of Materials Sciences and Engineering under Award No. DE-FG02-09ER46600. Research carried out in part at the Center for Functional Nanomaterials, Brookhaven National Laboratory, which is supported by the U.S. Department of Energy, Office of Basic Energy Sciences, under Contract No. DE-AC02-98CH10886.

[1]K. Mistry, C. Allen, C. Auth, B. Beattie, D. Bergstrom, M. Bost, M. Brazier, M. Buehler, A. Cappellani, R. Chau *et al.*, Tech. Dig. - Int. Electron Devices Meet. **2007**, 247.
[2]P. Bai, C. Auth, S. Balakrishnan, M. Bost, R. Brain, V. Chikarmane, R. Heussner, M. Hussein, J. Hwang, D. Ingerly *et al.*, Tech. Dig. - Int. Electron Devices Meet. **2004**, 657.
[3]J. Li, J. W. Mayer, and E. G. Colgan, J. Appl. Phys. **70**, 2820 (1991).
[4]X. Q. Wang, J. C. Hanson, A. I. Frenkel, J. Y. Kim, and J. A. Rodrigues, J. Phys. Chem. B **108**, 13667 (2004).
[5]T. Tabakova, V. Idakiev, J. Papavasiliou, G. Avgouropoulos, and T. Loannides, Catal. Commun. **8**, 101 (2007).
[6]J. A. Rodriguez, P. Liu, J. Hrbek, J. Evans, and M. Perez, Angew. Chem., Int. Ed. **46**, 1329 (2007).
[7]M. Turco, G. Bagnasco, U. Costantino, F. Marmottini, T. Montanari, G. Ramis, and G. Busca, J. Catal. **228**, 43 (2004).

[8]G. W. Zhou and J. C. Yang, Phys. Rev. Lett. **89**, 106101 (2002); J. Mater. Res. **20**, 1684 (2005); Appl. Surf. Sci. **210**, 165 (2003); Appl. Surf. Sci. **222**, 357 (2004); G. W. Zhou, L. L. Luo, L. Li, J. Ciston, E. A. Stach, and J. C. Yang, Phys. Rev. Lett. **109**, 235502 (2012).
[9]J. A. Eastman, P. H. Fuoss, L. E. Rehn, P. M. Baldo, G. W. Zhou, D. D. Fong, and L. J. Thompson, Appl. Phys. Lett. **87**, 051914 (2005).
[10]M. Lampimaki, K. Lahtonen, M. Hirsimaki, and M. Valden, J. Chem. Phys. **126**, 034703 (2007).
[11]M. Honkanen, M. Vippola, and T. Lepisto, J. Mater. Res. **23**, 1350 (2008).
[12]Y. Zhu, K. Mimura, and M. Isshiki, Oxid. Met. **62**, 207 (2004).
[13]Y. F. Zhu, K. Mimura, S. H. Hong, and M. Isshiki, J. Electrochem. Soc. **152**, B296 (2005).
[14]J. W. Lim, J. Iijima, Y. F. Zhu, J. H. Yoo, G. S. Choi, K. Mimura, and M. Isshiki, Thin Solid Films **516**, 4040 (2008).
[15]G. W. Zhou, L. Wang, R. C. Birtcher, P. M. Baldo, J. E. Pearson, J. C. Yang, and J. A. Eastman, Phys. Rev. Lett. **96**, 226108 (2006); G. W. Zhou, J. A. Eastman, R. C. Birtcher, P. M. Baldo, J. E. Pearson, L. J. Thompson, L. Wang, and J. C. Yang, J. Appl. Phys. **101**, 033521 (2007).
[16]G. W. Zhou and J. C. Yang, Phys. Rev. Lett. **93**, 226101 (2004); G. W. Zhou, W. Y. Dai, and J. C. Yang, Phys. Rev. B **77**, 245427 (2008).
[17]X. Duan, O. Warschkow, A. Soon, B. Delley, and C. Stampfl, Phys. Rev. B **81**, 075430 (2010).
[18]W. A. Saidi, M. Y. Lee, L. Li, G. W. Zhou, and A. J. H. McGaughey, Phys. Rev. B **86**, 245429 (2012).
[19]A. N. Aleshin, V. K. Egorov, B. S. Bokstein, and P. V. Kurkin, J. Appl. Phys. **77**, 6239 (1995).
[20]A. N. Aleshin, B. S. Bokstein, V. K. Egorov, and P. V. Kurkin, Defect Diffus. Forum **95–98**, 457 (1993).